The Astrophysical Journal, 630:535–542, 2005 September 1

PROPERTIES OF CENTRAL CAUSTICS IN PLANETARY MICROLENSING

Sun-Ju Chung,[1] Cheongho Han,[1,2] Byeong-Gon Park,[3] Doeon Kim,[1] Sangjun Kang,[4] Yoon-Hyun Ryu,[5]
Kang Min Kim,[3] Young-Beom Jeon,[3] Dong-Wook Lee,[6] Kyongae Chang,[7]
Woo-Baik Lee,[8] and Yong Hee Kang[9]

Received 2005 March 14; accepted 2005 May 17

ABSTRACT

To maximize the number of planet detections, current microlensing follow-up observations are focusing on high-magnification events that have a higher chance of being perturbed by central caustics. In this paper, we investigate the properties of central caustics and the perturbations that they induce. We derive analytic expressions for the location, size, and shape of the central caustic as a function of the star-planet separation, s, and the planet/star mass ratio, q, under the planetary perturbative approximation and compare the results with those based on numerical computations. While it has been known that the size of the planetary caustic is $\propto q^{1/2}$, we find from this work that the dependence of the size of the central caustic on q is linear, i.e., $\propto q$, implying that the central caustic shrinks much more rapidly with the decrease of q compared to the planetary caustic. The central caustic size also depends on the star-planet separation. If the size of the caustic is defined as the separation between the two cusps on the star-planet axis (horizontal width), we find that the dependence of the central caustic size on the separation is $\propto(s + s^{-1})$. While the size of the central caustic depends both on s and on q, its shape, defined as the vertical/horizontal width ratio, $\mathcal{R}_c$, is solely dependent on the planetary separation, and we derive an analytic relation between $\mathcal{R}_c$ and s. Due to the smaller size of the central caustic, combined with a much more rapid decrease of its size with the decrease of q, the effect of finite source size on the perturbation induced by the central caustic is much more severe than the effect on the perturbation induced by the planetary caustic. As a result, we find that although giant planets with $q \gtrsim 10^{-3}$ can be detected from the planet-search strategy of monitoring high-magnification events, detecting signals of Earth-mass planets with $q \sim 10^{-5}$ will be very difficult. Although the central caustics of a pair of planets with separations s and s^{-1} are identical to linear order, we find that the magnification patterns induced by a pair of degenerate caustics of planets with $q \gtrsim 10^{-3}$ are different to the level of being noticed in observations with $\lesssim$2% photometry. Considering that the majority of planets that would be detected by the strategy of monitoring high-magnification events are giant planets, we predict that the $s \leftrightarrow s^{-1}$ degeneracy could be broken for a majority of planetary events from observations with good enough precision.

Subject headings: gravitational lensing — planetary systems — planets and satellites: general

Online material: color figures

1. INTRODUCTION

Various methods have been proposed to detect and characterize extrasolar planets, including the radial velocity technique (Mayor & Queloz 1995; Marcy & Butler 1996), the transit method (Struve 1952), direct imaging (Angel 1994; Stahl & Sandler 1995), pulsar timing analysis (Wolszczan & Frail 1992), and microlensing (Mao & Paczyński 1991; Gould & Loeb 1992). (See also the review of Perryman [2000].) The microlensing signal of a planetary companion to Galactic disk and bulge microlens stars is the short-duration perturbation to the smooth standard light curve of the primary-induced lensing event that occurred on a background star. Compared to other methods, the decay of the planetary lensing signal with the decrease of the planet/star mass ratio is relatively slow, and thus the microlensing technique has an important advantage of being applicable to detecting Earth-mass planets using an already existing instrument (Bennett & Rhie 1996). The microlensing method also has a unique applicability to the detections of free-floating planets (Bennett & Rhie 2002; Han et al. 2004, 2005). In addition, the method is not restricted to planets of nearby stars and can be extended even to nearby galaxies (Baltz & Gondolo 2001). Recently, two clear-cut microlensing detections of exoplanets were reported by Bond et al. (2004) and Udalski et al. (2005).

Due to the rare and incidental chance of lensing events, combined with the short duration of planet signals, planetary lensing searches require a special observational setup, in which survey observations issue alerts of ongoing events in the early stage of lensing magnification (Soszyński et al. 2001; Bond et al. 2001) and follow-up collaborations intensively monitor the alerted events (Bond et al. 2002; Park et al. 2004; Cassan et al. 2004). However, follow-up is generally done with an instrument with a small field of view, and thus events are monitored sequentially. As a result, only a handful of events can be followed at any given time, limiting the number of planet detections. To

[1] Department of Physics, Institute for Basic Science Research, Chungbuk National University, Chongju 361-763, South Korea; cheongho@astroph.chungbuk.ac.kr.
[2] Corresponding author.
[3] Bohyunsan Optical Astronomy Observatory, Korea Astronomy and Space Science Institute, Youngchon 770-820, South Korea.
[4] School of Liberal Arts, Semyung University, Jechon 390-711, South Korea.
[5] Department of Astronomy and Atmospheric Sciences, Kyungpook National University, Daegu 702-701, South Korea.
[6] Astrophysical Research Center for the Structure and Evolution of the Cosmos, Sejong University, Seoul 143-747, South Korea.
[7] Department of Computer and Applied Physics, Chongju University, Chongju 360-764, South Korea.
[8] Korea Astronomy and Space Science Institute, Taejon 305-348, South Korea.
[9] Department of Earth Science Education, Kyungpook National University, Daegu 702-701, South Korea.

maximize the number of potential planet detections with a limited use of resources and time, Griest & Safizadeh (1998) proposed focusing on high-magnification events. They pointed out that high-magnification events have a dramatically higher chance of being perturbed by planets due to the existence of a "central" caustic (see § 2 for more details). By adopting this proposal, current follow-up experiments are giving high priority to these events (Albrow et al. 2001; Rattenbury et al. 2002; Bond et al. 2002; Abe et al. 2004; Jiang et al. 2004). However, little has been studied about the characteristics of central caustics and the perturbations induced by them (central perturbations).

In this paper, we investigate the properties of central caustics and the perturbations that they induce. The layout of the paper is as follows. In § 2, we describe basic physics of planetary lensing. In § 3, we analytically investigate how the location, size, and shape of the central caustic vary depending on the mass ratio, q, and separation, s, of the planets under the planetary perturbative approximation and compare the results with those based on numerical computations. In § 4, we then systematically inspect the patterns of central perturbations by constructing maps of magnification excess for planets with various values of s and q. From the constructed maps, we also examine the effect of finite source size and investigate the possible types of planets detectable for given source stars with various sizes. We summarize the results and conclude in § 5.

2. BASICS OF PLANETARY LENSING

The lensing mapping from the lens plane to the source plane of N point masses with no external shear or convergence is described by the lens equation

$$\zeta = z - \sum_{j=1}^{N} \frac{m_j/M}{\bar{z} - \bar{z}_{L,j}}, \tag{1}$$

where $\zeta = \xi + i\eta$, $z_{L,j} = x_{L,j} + iy_{L,j}$, and $z = x + iy$ are the complex notations of the source, lens, and image positions, respectively, $\bar{z}$ denotes the complex conjugate of z, m_j are the masses of the individual lens components, and $M = \sum_j m_j$ is the total mass of the lens system (Witt 1990). Here all angles are normalized to the Einstein ring radius $\theta_{\rm E}$ of the total mass of the system, i.e.,

$$\theta_{\rm E} = \frac{r_{\rm E}}{D_L} = \left[\frac{4GM}{c^2}\left(\frac{1}{D_L} - \frac{1}{D_S}\right)\right]^{1/2}, \tag{2}$$

where D_L and D_S are the distances to the lens and source, respectively. For a single lens ($N = 1$), there exist two images with locations at $u_{I,\pm} = 0.5[u \pm (u^2 + 4)^{1/2}]$ and magnifications of $A_\pm = 0.5(A \pm 1)$, where $u \equiv |\zeta - z_L|$ is the separation between the lens and source. Then the total magnification corresponds to the sum of the magnifications of the individual images and is related to u by

$$A = A_+ + A_- = \frac{(u^2 + 2)}{u(u^2 + 4)^{1/2}}. \tag{3}$$

A planetary lensing is described by the formalism of a binary ($N = 2$) lens with a very low mass companion. For a binary lens, there are three or five images, and the number of images changes by two as the source crosses a caustic. The caustics are important features of binary lensing and represent the set of source positions at which the magnification of a point source becomes infinite. The caustics of binary lensing form single or multiple closed figures, where each figure is composed of concave curves (fold caustics) that meet at cusps. For a planetary case, there exist two sets of disconnected caustics: one "central caustic" located close to the host star and one or two "planetary caustics," depending on whether the planet lies outside or inside the Einstein ring. Since the central caustic lies close to the host star, the perturbation induced by the central caustic occurs close to the peak of the lensing light curves of high-magnification events. For a star-planet system, it is known that the lensing behavior can be described by the perturbation approach because of the small planet/star mass ratio (Bozza 1999; Asada 2002; An 2005). In this case, the lensing equation is expressed as

$$\zeta = z - 1/\bar{z} - q/(\bar{z} - \bar{z}_p), \tag{4}$$

where the position of the star is chosen as the coordinate origin and z_p represents the location of the planet.

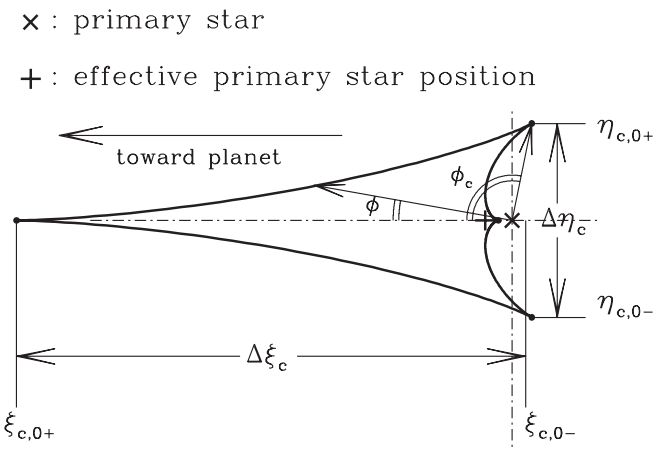

FIG. 1.—Geometry of a central caustic. [*See the electronic edition of the Journal for a color version of this figure.*]

3. PROPERTIES OF CENTRAL CAUSTICS

Under the planetary perturbative approximation ($q \ll 1$ and $||z_p| - 1| \gg q$), the location of the central caustic can be expressed in an analytic form (An 2005),

$$\zeta_c \simeq \frac{q}{2} e^{i\phi}\left[\frac{1}{(1 - z_p e^{-i\phi})^2} + \frac{1}{(1 - \bar{z}_p^{-1} e^{-i\phi})^2} - 1\right], \tag{5}$$

where the polar coordinates are centered at the position of the primary star and ϕ represents the polar angle (see Fig. 1). With the notation for the star-planet separation of $s = |z_p|$, the caustic position is expressed in an explicit form,

$$\xi_c \simeq \frac{s + s^{-1} + 2(\cos^3\phi - 2\cos\phi)}{(s + s^{-1} - 2\cos\phi)^2} q, \tag{6}$$

$$\eta_c \simeq -\frac{2\sin^3\phi}{(s + s^{-1} - 2\cos\phi)^2} q. \tag{7}$$

The central caustic has an elongated asteroid shape with four cusps, where two of them are located on the star-planet axis and the other two are located off the axis. Cusps of a central caustic occur when $d\zeta_c/d\phi = 0$ (i.e., when $\phi = 0$ and π for the on-axis

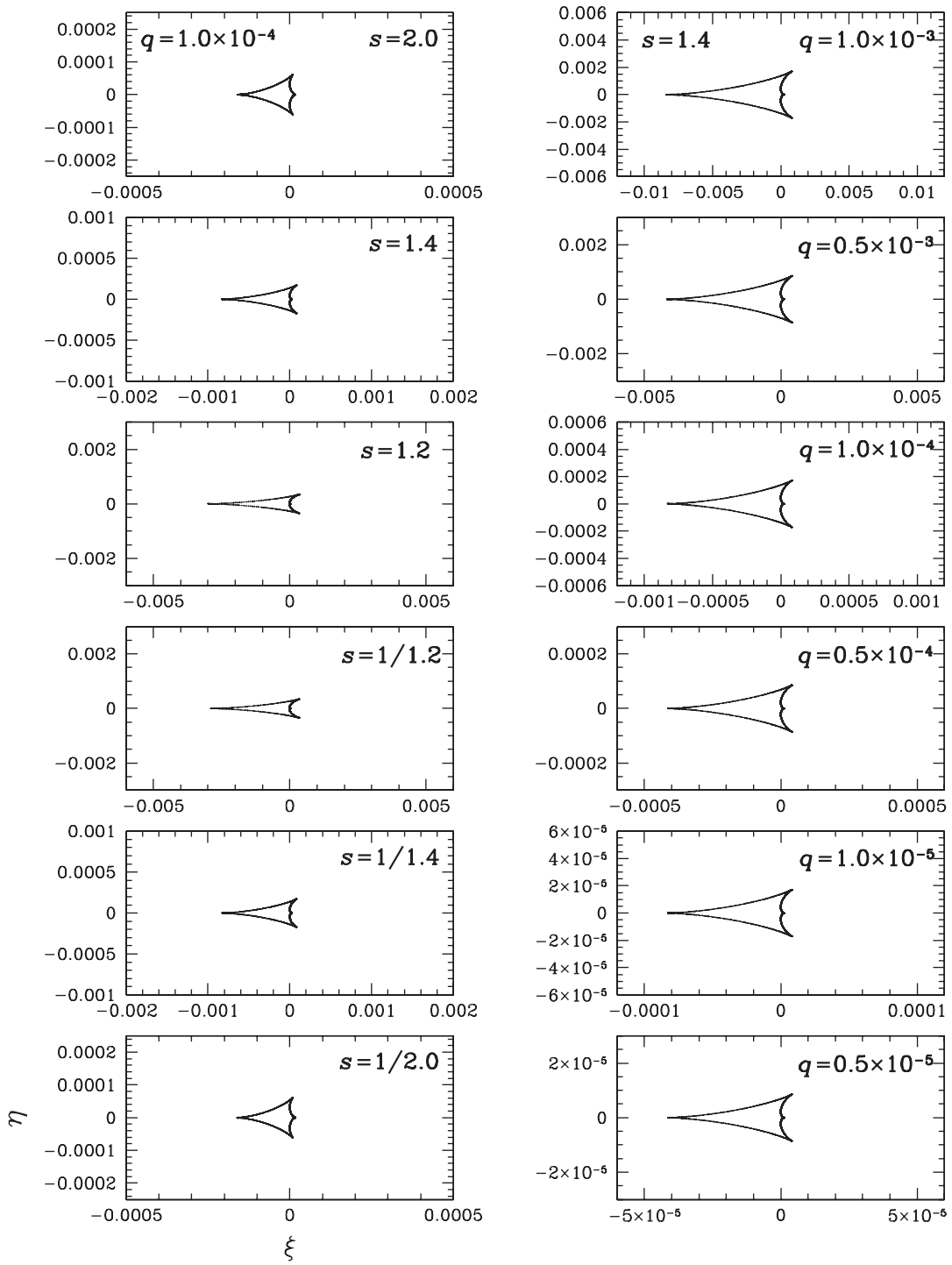

FIG. 2.—Variations of the shape and size of the central caustic produced by planets with various separations from and mass ratios relative to the primary star. The left panels show the variations of the shape of the central caustic depending on the separation, while the right panels show the variation depending on the mass ratio. In all cases, coordinates are centered at the *effective* position of the host star, and the planets are located on the left side. Note that the axis scales differ from one panel to another for better comparison of the caustic shapes. [*See the electronic edition of the Journal for a color version of this figure.*]

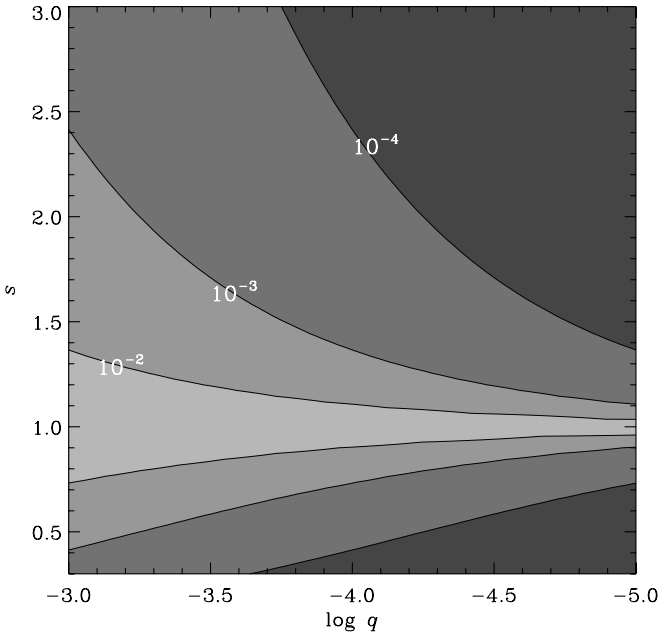

FIG. 3.—Size of the central caustic, as measured by the horizontal width, as a function of s and q.

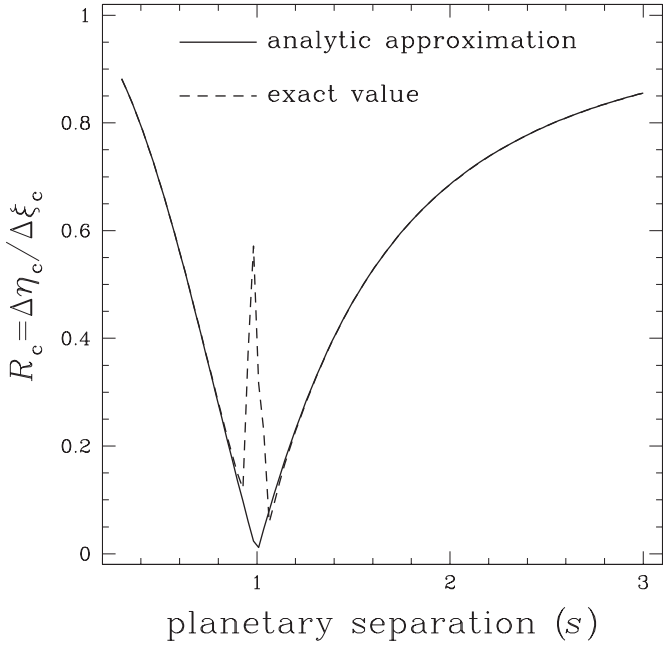

FIG. 4.—Dependence of the central caustic shape, as measured by the ratio between horizontal and vertical widths, on the planet-star separation. The computations are based on planets with $q = 10^{-4}$. [*See the electronic edition of the Journal for a color version of this figure.*]

cusps and when $\phi = \phi_c$ and $2\pi - \phi_c$ for the off-axis cusps), and thus their locations are found to be

$$\xi_{c,0\pm} \simeq \pm \frac{q}{(1 \pm s)(1 \pm s^{-1})}, \tag{8}$$

$$\eta_{c,0\pm} \simeq \pm \frac{2q|\sin^3\phi_c|}{(s + s^{-1} - 2\cos\phi_c)^2}, \tag{9}$$

where

$$\cos\phi_c = \frac{3}{4}\left(s + \frac{1}{s}\right)\left[1 - \sqrt{1 - \frac{32}{9}\left(s + \frac{1}{s}\right)^{-2}}\right]. \tag{10}$$

Then the horizontal and vertical widths of the central caustic, defined as the separations between the on- and off-axis cusps (see Fig. 1), are, respectively,

$$\Delta\xi_c \simeq \left|\xi_{c,0+} - \xi_{c,0-}\right| = \frac{4q}{(s - s^{-1})^2}, \tag{11}$$

$$\Delta\eta_c \simeq \left|\eta_{c,0+} - \eta_{c,0-}\right| = \Delta\xi_c \frac{(s - s^{-1})^2|\sin^3\phi_c|}{(s + s^{-1} - 2\cos\phi_c)^2}. \tag{12}$$

In Figure 2, we present central caustics produced by planets with various separations and mass ratios. From the figure and equations (5)–(12), we find the following characteristics of the central caustic.

1. The size of the central caustic depends on both the separation and the mass ratio. The dependence of the central caustic size on the mass ratio is linear, i.e., $\propto q$, as shown in equations (5)–(7) and demonstrated in the right panels of Figure 2. By comparison, the size of the planetary caustic is proportional to $q^{1/2}$. This implies that the central caustic shrinks much more rapidly with the decrease of the planet mass compared to the planetary caustic. If the caustic size is defined as the horizontal width, then the size depends on the star-planet separation by $\Delta\xi_c \propto (s + s^{-1})^{-2}$. Then the caustic size becomes maximum when $s \sim 1$ and decreases with the increase of $|s - 1|$. In the limiting cases of a very wide separation planet ($s \gg 1$) and a close-in planet ($s \ll 1$), the dependences are, respectively,

$$\Delta\xi_c \propto \begin{cases} s^{-2} & \text{for } s \gg 1, \\ s^2 & \text{for } s \ll 1. \end{cases} \tag{13}$$

In Figure 3, we present the size of the central caustic as a function of s and q.

2. For a given mass ratio, a pair of central caustics with separations s and s^{-1} are identical to linear order. This can be seen from the pair of caustics with separations s and s^{-1} presented in Figure 2. Analytically, this can also be proved from equations (5)–(7), where the inversion of $s \leftrightarrow s^{-1}$ results in the same expression.

3. Under the perturbative approximation, the shape of the central caustic is solely dependent on the planet separation. We quantify the caustic shape as the vertical/horizontal width ratio, $\mathcal{R}_c = \Delta\eta_c/\Delta\xi_c$, and present the variation of $\mathcal{R}_c$ as a function of s in Figure 4. In the figure, we present two curves: one is based on the perturbative approximation, and the other is based on numerical computation. One finds that the width ratios based on the analytic and numerical computations match very well, except the region around $s \sim 1$, where the perturbative approximation is not valid. We find that the difference in this region is caused by the merge of the planetary and central caustics.[10] One also finds that the width ratio of the central caustic rapidly increases with the decrease of $|s - 1|$.

4. CENTRAL CAUSTIC PERTURBATIONS

Knowing now the characteristics of central caustics, we then investigate the pattern of planetary perturbations induced by

[10] The planetary caustic produced by a planet with a separation s from its parent star is located at $\boldsymbol{x}_{\rm pc} \sim \boldsymbol{s} - 1/\boldsymbol{s}$. Therefore, as $s \to 1$, $x_{\rm pc} \to 0$, and thus the planetary caustic approaches the central caustic and eventually merges with it.

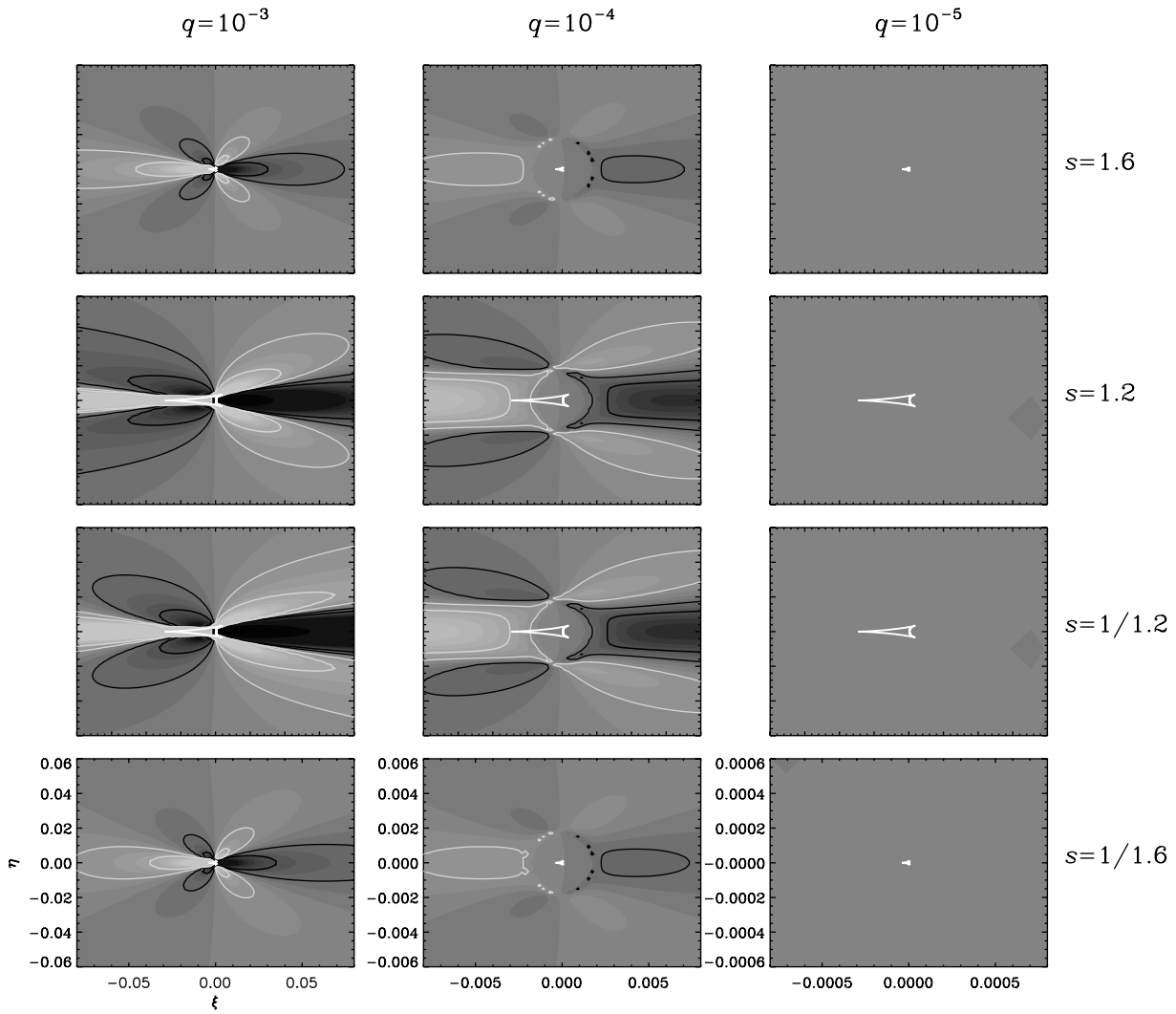

FIG. 5.—Contour maps of magnification excess as a function of source position (ξ, η) for planetary lens systems with various star-planet separations and planet/star mass ratios in the region around the central caustics. Contours are drawn at the levels of $\epsilon = \pm 2\%$ (*thin curves*) and $\pm 5\%$ (*thick curves*), and a gray scale is used to represent positive (*light*) and negative (*dark*) deviation regions. All lengths are scaled by the Einstein ring radius corresponding to the total mass of the lens system. The coordinates are centered at the effective position of the host star. In all cases, planets are located on the left side. The maps are constructed for a main-sequence source star with a normalized radius of $\rho_\star = 0.0018$, which corresponds to the case in which the source with an absolute radius of $R_\star = 1\ R_\odot$ and located at $D_S = 8$ kpc is lensed by a lens with $m = 0.3\ M_\odot$ and $D_L = 6$ kpc.

central caustics. For this purpose, we construct maps of magnification excess, which is defined as

$$\epsilon(\xi, \eta) = \frac{A - A_0}{A_0}, \tag{14}$$

where A is the exact magnification of the planetary lensing and A_0 is the single-lensing magnification caused by the host star at its "effective" position. Due to the additional deflection of light produced by the presence of the companion, it was known that the effective lensing position of a component of the binary lens system is shifted toward its companion (Di Stefano & Mao 1996; An & Han 2002). The amount of the shift of a lens component i toward the other component j is

$$\Delta x_{L,i\to j} \simeq \frac{m_j/m_i}{(s + s^{-1})/(\theta_{\mathrm{E},i}/\theta_{\mathrm{E}})} \frac{\theta_{\mathrm{E},i}}{\theta_{\mathrm{E}}}, \tag{15}$$

where m_i and m_j are the masses of the individual lens components and $\theta_{\mathrm{E},i}$ is the Einstein ring radius corresponding to m_i (An & Han 2002). For a planetary lens case, the shift of the host star (with the notation "$\star$") toward the planet (with the notation "p") is expressed as

$$\Delta x_{L,\star\to p} \simeq \frac{q}{(s + s^{-1})}, \tag{16}$$

because $\theta_{\mathrm{E},\star} \sim \theta_{\mathrm{E}}$ and $m_p/m_\star = q$.[11] Then as either $|s - 1| \to \infty$ (wide-separation planet) or $|s - 1| \to 0$ (close-in planet), the shift is $\Delta x_{L,\star\to p} \to 0$, and thus the effective lensing position of the primary star approaches its original position.

In Figures 5–7, we present the constructed magnification-excess maps for planets with various values of s and q. Planetary signal is important for planets with separations within the so-called lensing zone of $1/1.6 \lesssim s \lesssim 1.6$ (Gould & Loeb 1992), and thus we plot maps for planets located within this range. To

[11] We note that the term s^{-1} in eqs. (15) and (16) was not included in the corresponding equations of Di Stefano & Mao (1996) and An & Han (2002), where they treated only wide-separation binaries. We introduce this term to keep the symmetry between the central caustics of planets with separations s and s^{-1}.

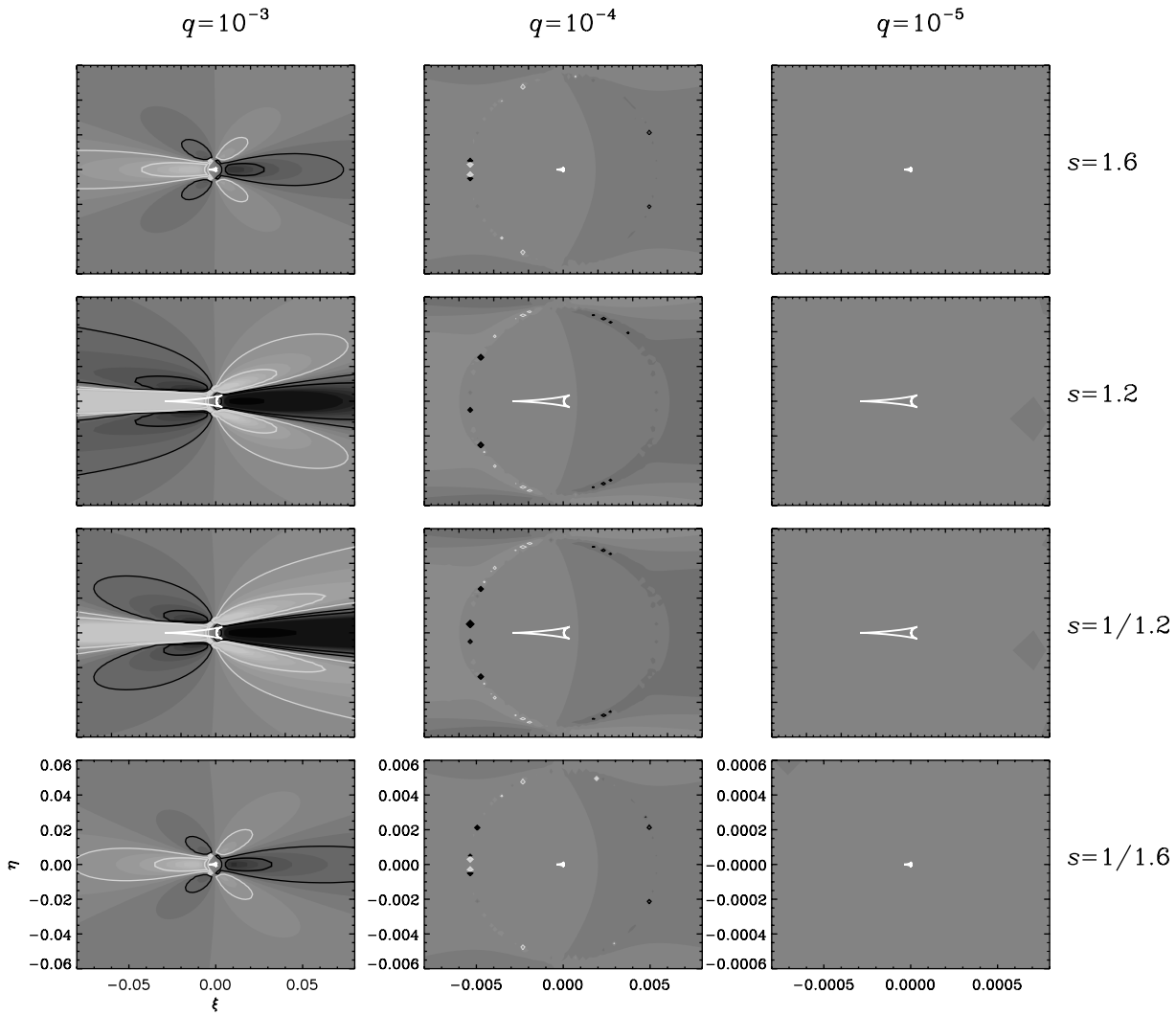

FIG. 6.—Contour maps of magnification excess for the same planetary lens systems as in Fig. 5, but for events associated with a turnoff source star with $\rho_\star = 0.0054$.

see the effect of finite source size, we construct three sets of maps with main-sequence (with a radius of $R_\star = 1\ R_\odot$), turnoff (with $R_\star = 3\ R_\odot$), and clump giant (with $R_\star = 13\ R_\odot$) source stars; they are presented in Figures 5, 6, and 7, respectively. The magnification of a finite source with a surface brightness profile of $I(\boldsymbol{\zeta})$ is computed by the intensity-weighted magnification averaged over the source-star surface, i.e.,

$$A_{\rm fs}(\boldsymbol{\zeta}) = \frac{\int_S I(\boldsymbol{\zeta}')A(\boldsymbol{\zeta}+\boldsymbol{\zeta}')\,d\boldsymbol{\zeta}'}{\int_S I(\boldsymbol{\zeta}')\,d\boldsymbol{\zeta}'}, \qquad (17)$$

where A denotes the point-source magnification, $\boldsymbol{\zeta}$ is the vector position of the center of the source, $\boldsymbol{\zeta}'$ is the displacement vector of a point on the source-star surface with respect to the source star's center, and the two-dimensional integral is over the source-star surface S. The effect of finite source size is smearing out the detailed structures of the planetary lensing signals. The finite-source effect is determined by the *normalized* source radius $\rho_\star$, which represents the angular radius of a star, $\theta_\star$, in units of the Einstein ring radius, i.e., $\rho_\star = \theta_\star/\theta_{\rm E}$. We thus set $\rho_\star$ of the individual stars by choosing an Einstein radius of $\theta_{\rm E} = 0.32$ mas that corresponds to the value of the most frequent Galactic bulge event with $m = 0.3\ M_\odot$, $D_L = 6$ kpc, and $D_S = 8$ kpc. Then the normalized source radius of a $R_\star = 1\ R_\odot$ star corresponds to $\rho_\star = 0.0018$. For a source with uniform surface brightness, the computation can be reduced from a two-dimensional to a one-dimensional integral using the generalized Stokes theorem (Gould & Gaucherel 1997; Dominik 1998). To accelerate computations, we thus assume that the source stars have uniform surface brightness. However, we note that the effect of nonuniform surface brightness on the planetary lensing signal is not important. For a planetary system with a primary star of $m = 0.3\ M_\odot$, the mass ratios of Jupiter-, Saturn-, Neptune-, and Earth-mass planets correspond to $q \sim 3\times10^{-3}$, 10^{-3}, 10^{-4}, and 10^{-5}, respectively.

From the excess maps, we find the following properties of central perturbations.

1. We find that the effect of finite source size on central perturbations is much more severe than the effect on perturbations caused by planetary caustics. This is because the central caustic is not only much smaller but also shrinks much more rapidly with the decrease of q than the planetary caustic. As a result, we find that although giant planets with $q \gtrsim 10^{-3}$ can be detected by the planet-search strategy of monitoring high-magnification events, detecting signals of Earth-mass planets with $q \sim 10^{-5}$ would be very difficult. It is estimated that the lower mass limit of detectable planets will be that of a Neptune-mass planet with

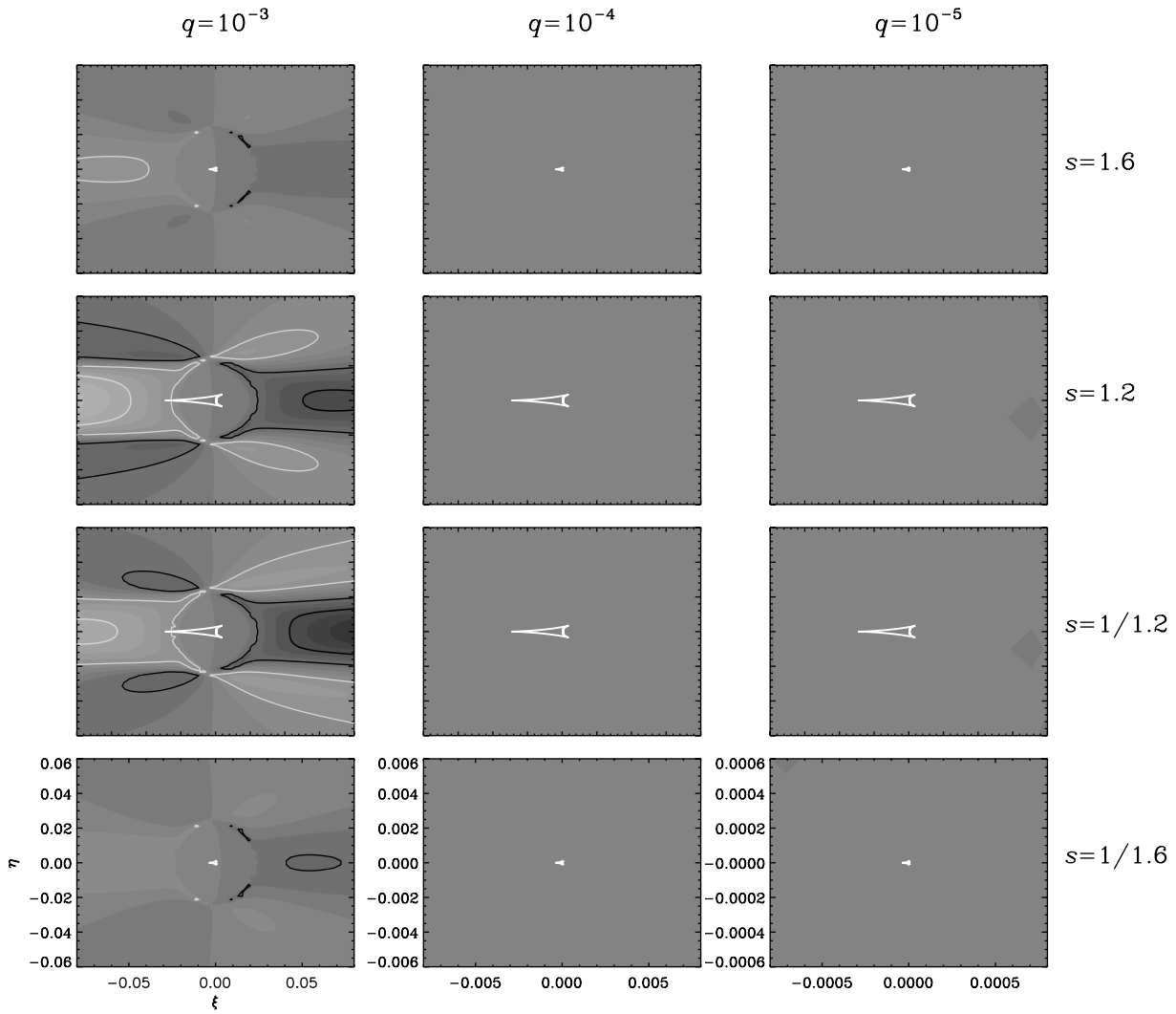

FIG. 7.—Contour maps of magnification excess for the same planetary lens systems as in Fig. 5, but for events associated with a clump giant with $\rho_\star = 0.0234$.

TABLE 1
DETECTABILITY OF PLANETARY SIGNALS

Source Type	Detectability
$q = 10^{-3}$	
Main sequence ($\rho_\star = 0.0018$)	O
Turnoff ($\rho_\star = 0.0054$)	O
Clump giant ($\rho_\star = 0.0234$)	O
$q = 10^{-4}$	
Main sequence ($\rho_\star = 0.0018$)	O
Turnoff ($\rho_\star = 0.0054$)	△
Clump giant ($\rho_\star = 0.0234$)	X
$q = 10^{-5}$	
Main sequence ($\rho_\star = 0.0018$)	X
Turnoff ($\rho_\star = 0.0054$)	X
Clump giant ($\rho_\star = 0.0234$)	X

NOTES.—The adopted source radii are $R_\star = 1$, 3, and 13 $R_\odot$ for the main-sequence, turnoff, and clump giant stars, respectively. The normalized source radius $\rho_\star = \theta_\star/\theta_{\rm E}$ of each source star is determined by choosing an Einstein ring radius of $\theta_{\rm E} = 0.32$ mas that corresponds to the value of the most frequent Galactic bulge event with $m = 0.3\ M_\odot$, $D_L = 6$ kpc, and $D_S = 8$ kpc. The individual symbols for the detectability represent possible (O), marginal (△), and very difficult (X).

$q \sim 10^{-4}$, but detecting planets in this mass range would be possible only for events associated with source stars smaller than turnoff stars. In Table 1, we summarize the possible types of planets detectable from events involved with various types of source stars.

2. As expected by the close similarity between the pair of caustics with separations s and s^{-1}, the pattern of perturbations induced by these two caustics are similar to each other. A good example is the pair of maps with $(s, q) = (1.2, 10^{-4})$ and $(1/1.2, 10^{-4})$ in Figure 5. However, we find that as the planet mass increases, the difference between the perturbation patterns of the pair of planets increases. We find that the difference is large enough to be noticed for planets with $q \gtrsim 10^{-3}$, e.g., the pair of maps of the planets with $(s, q) = (1.2, 10^{-3})$ and $(1/1.2, 10^{-3})$. Considering that the majority of planets detectable by the strategy of monitoring high-magnification events are giant planets, we predict that the $s \leftrightarrow 1/s$ degeneracy could be broken for a majority of planetary events from observations with a $\lesssim$2% photometric precision.

5. SUMMARY AND CONCLUSION

We investigated the properties of central caustics and the perturbations induced by them. Under the planetary perturbative approximation, we derived analytic expressions for the location,

size, and shape of the central caustic as a function of the planet separation and mass ratio and compared the results with those based on numerical computations. While it has been known that the size of the planetary caustic is proportional to $q^{1/2}$, we found from this work that the dependence of the central caustic size on the mass ratio is linear. As a result, the central caustic shrinks much more rapidly with the decrease of the planet mass, compared to the planetary caustic. Due to the large finite-source effect caused by the smaller size of the central caustic, combined with the much more rapid decrease of its size with the decrease of q, we predict that although giant planets with $q \gtrsim 10^{-3}$ can be detected by the planet-search strategy of monitoring high-magnification events, detecting signals of Earth-mass planets with $q \sim 10^{-5}$ would be very difficult. Although the central caustics of a pair of planets with separations s and s^{-1} are identical to linear order, we found that the difference between the magnification patterns induced by the pair of degenerate caustics of planets with $q \gtrsim 10^{-3}$ can be noticed at the level of $\sim$2%. Because the majority of planets expected to be detected by the strategy of monitoring high-magnification events are giant planets, we predict that the $s \leftrightarrow s^{-1}$ degeneracy could be broken for a majority of planetary events from observations with good enough photometric precision.

We would like to thank J. H. An for making helpful comments. Work by C. H. was supported by the Astrophysical Research Center for the Structure and Evolution of the Cosmos (ARCSEC) of the Korea Science and Engineering Foundation (KOSEF) through the Science Research Program (SRC) program. B.-G. P. acknowledges support from a grant of the Korea Astronomy and Space Science Institute (KASI).

REFERENCES

Abe, F., et al. 2004, Science, 305, 1264
Albrow, M. D., et al. 2001, ApJ, 556, L113
An, J. H. 2005, MNRAS, 356, 1409
An, J. H., & Han, C. 2002, ApJ, 573, 351
Angel, J. R. P. 1994, Nature, 368, 203
Asada, H. 2002, ApJ, 573, 825
Baltz, E. A., & Gondolo, P. 2001, ApJ, 559, 41
Bennett, D. P., & Rhie, S. H. 1996, ApJ, 472, 660
———. 2002, ApJ, 574, 985
Bond, I. A., et al. 2001, MNRAS, 327, 868
———. 2002, MNRAS, 333, 71
———. 2004, ApJ, 606, L155
Bozza, V. 1999, A&A, 348, 311
Cassan, A., et al. 2004, A&A, 419, L1
Di Stefano, R., & Mao, S. 1996, ApJ, 457, 93
Dominik, M. 1998, A&A, 333, L79
Gould, A., & Gaucherel, C. 1997, ApJ, 477, 580
Gould, A., & Loeb, A. 1992, ApJ, 396, 104
Griest, K., & Safizadeh, N. 1998, ApJ, 500, 37
Han, C., Chung, S.-J., Kim, D., Park, B.-G., Ryu, Y.-H., Kang, S., & Lee, D. W. 2004, ApJ, 604, 372
Han, C., Gaudi, B. S., An, J. H., & Gould, A. 2005, ApJ, 618, 962
Jiang, G., et al. 2004, ApJ, 617, 1307
Mao, S., & Paczyński, B. 1991, ApJ, 374, L37
Marcy, G. W., & Butler, R. P. 1996, ApJ, 464, L147
Mayor, M., & Queloz, D. 1995, Nature, 378, 355
Park, B.-G., et al. 2004, ApJ, 609, 166
Perryman, M. A. C. 2000, Rep. Prog. Phys., 63, 1209
Rattenbury, N. J., Bond, I. A., Skuljan, J., & Yock, P. C. M. 2002, MNRAS, 335, 159
Soszyński, I., et al. 2001, ApJ, 552, 731
Stahl, S. M., & Sandler, D. G. 1995, ApJ, 454, L153
Struve, O. 1952, Observatory, 72, 199
Udalski, A., et al. 2005, ApJ, 628, L109
Witt, H. J. 1990, A&A, 236, 311
Wolszczan, A., & Frail, D. A. 1992, Nature, 355, 145